J Electroceram (2016) 36:46–57
DOI 10.1007/s10832-016-0024-3

Dielectric properties of pure and Mn-doped $CaCu_3Ti_4O_{12}$ ceramics over a wide temperature range

ChunChang Wang[1] · Wei Ni[1] · Da Zhang[1] · Xiaohong Sun[1] · Jing Wang[1] · Haibo Li[1] · Nan Zhang[1]

Received: 4 November 2015 / Accepted: 1 March 2016 / Published online: 8 March 2016

Abstract The effect of manganese doping on the dielectric properties of $CaCu_3Ti_{4-x}Mn_xO_{12}$ (x = 0, 0.02, 0.04) were investigated over a broad temperature range (93–723 K) in the frequency range from 100 Hz to 10 MHz. Two dielectric relaxations and two dielectric anomalies were observed. The low-temperature relaxation appearing in the temperature range below 200 K is the characteristic relaxation for $CaCu_3Ti_4O_{12}$. This relaxation was attributed to the polaron relaxation due to electron hopping between Ti^{3+} and Ti^{4+} states. Due to the negative factors of notable decreases in the Ti^{3+}/Ti^{4+} and Cu^{3+}/Cu^{2+} ratios and the concentration of oxygen vacancies as revealed by X-ray photoemission spectroscopy, Mn-doping was found to gradually destroy rather than move this relaxation to a higher temperature. The high-temperature relaxation occurring around room temperature was found to be a Maxwell-Wagner relaxation caused by grain boundaries. Our results confirm that the colossal dielectric behavior in the tested samples results from both polaron and Maxwell-Wagner relaxations, but is predominated by the latter relaxation. The low-temperature anomaly behaves as a phase-transition-like behavior. It was argued to be created by oxygen vacancies transition from static disorder to dynamic disorder. The high-temperature anomaly is an artificial effect caused by negative capacitance.

Keywords CCTO · Dielectric properties · High-temperature · Artificial effect

✉ ChunChang Wang
ccwang@ahu.edu.cn

[1] Laboratory of Dielectric Functional Materials, School of Physics & Material Science, Anhui University, Hefei 230601, China

1 Introduction

Since the discovery of colossal dielectric constant (CDC) effect in $CaCu_3Ti_4O_{12}$ (CCTO) ceramics in 2000, a burst of research activities on this effect has been stimulated [1]. The characteristic feature for CDC behavior is that there exists a dielectric constant (ε') sigmoidal between two dielectric plateaus accompanied by a Debye-like peak in the corresponding dielectric loss. Although the extrinsic origin of Maxwell–Wagner relaxation resulting from spatial inhomogeneity, contact effect, and internal barrier layer capacitor is generally accepted to be the cause of the CDC behavior of CCTO, an intrinsic relaxation mechanism for the CDC effect is still active [2–5]. For example, earlier researches on CCTO suggested that the local dipoles induced by Ti displacement could be responsible for the high permittivity [6, 7]. Recent researches revealed that the mixed-valent structure (e.g., Ti^{3+}/Ti^{4+}, Fe^{2+}/Fe^{3+}, Cu^{+}/Cu^{2+}, Mn^{3+}/Mn^{4+}, and so on) correlated with oxygen vacancies is a common feature for CDC materials [8–17]. This feature further leads to the two characteristic natures for CDC behavior: on one hand, the electrons created by the ionization of the oxygen vacancies can hop between the mixed-valent ions giving rise to the polaronic nature of the relaxation for the behavior [16]; on the other hand, electron-ordering on the mixed-valent ions yields the nature similar to electronic ferroelectricity for the behavior [9]. These natures make the CDC behavior very sensitive to sintering conditions, post-sintering annealing treatments, and element doping effects, as these facts can affect either the concentration of oxygen vacancies, or the ratio of mixed-valent ions, or both [18–23].

Among different dopants, Mn is seriously harmful to the CDC behavior. It was reported that a low doping level of 2 % substitution of Mn for the multivalent cations Cu or Ti can completely eliminate the CDC behavior [20, 21]. The effect of

Mn doping was believed to greatly reduce the Schottky barrier height at the grain boundary [24]. However, Kim and coauthors reported that the Mn doping plays significant role in adjusting the ratio of Cu/Ca [25]. Based on the above point that the CDC behavior is related to the mixed-valent ions, it is naturally to suggest that Mn doping might result in a great reduction in the ratio of mixed-valent ions, thereby destructing the CDC behavior. However, as clued by the results reported in Ref. [26] that the dielectric constant sigmoidal of the 1 % Mn-doped sample appears around 350 K, which is much higher than ~50 K for the pure sample. This fact strongly implies that, instead of disappearance, the CDC behavior for Mn-doped samples might move toward a higher temperature above room temperature. Truly, the polaron relaxation due to electrons hopping between Mn^{3+} and Mn^{4+} ions was reported to occur at temperatures higher than room temperature [27]. Therefore, the role of the Mn-doping effects is still unclear.

We, herein, present a comparative study on the CDC behavior of the pure and Mn-doped CCTO ceramics over a broad temperature range of 93–723 K aiming at deeply understanding the role of the Mn-doping effects and the physical origin of the CDC behavior.

2 Experimental details

The nominally pure and doped CCTO ceramics by substituting 2 and 4 at.% Mn at Ti sites (abbreviated as CCTO, CCTMO-2, and CCTMO-4, respectively) were prepared using the conventional solid-state reaction method. High-purity (99.99 %) $CaCO_3$, CuO, TiO_2, and MnO_2 were thoroughly mixed and calcined at 950 °C in air for 5 h and 1100 °C for 10 h with intermediate grinding. The resultant materials were reground, then pressed into pellets of 12 mm in diameter and 1–2 mm in thickness under a pressure of 20 MPa, and finally sintered at 1100 °C for 10 h. Phase purity of the sintered pellets was characterized by X-ray powder diffraction (XRD) on a MXP18AHF diffractometer (Mac Science Co. Ltd, Yokohama, Japan) with Cu $K\alpha$ radiation ($\lambda = 1.5406$ Å). Microstructure and grain size of the sintered pellets were studied by a field-emission scanning electron microscope (SEM) (Model S-4 800, Hitachi Co. Ltd, Tokyo, Japan). X-ray photoemission spectroscopy (XPS) experiments were carried out on a Thermo ESCALAB 250 with Al Kα radiation ($h\nu = 1486.6$ eV). For dielectric characterization, pellets were printed with silver paste on both sides and then fired at 600 °C for 2 h in order to remove the polymeric component. The temperature-dependent dielectric properties were obtained using a Wayne Kerr 6500B precise impedance analyzer with the sample mounted in a holder placed inside a PST-2000HL dielectric measuring system. The temperature variations were automatically controlled using a Stanford temperature controller with a heating rate of 2 K/min. The ac measuring signal was 100 mV rms.

3 Results and discussion

3.1 Structure and microstructure characterization

Figure 1 presents XRD patterns of CCTO, CCTMO-2 and CCTMO-4. The diffraction patterns for the three samples are identified to be single cubic perovskite structure. The lattice constants of samples were calculated with Jade 5.0 software and found to be 7.3835(1), 7.3815(2), and 7.3784(9) Å for CCTO, CCTMO-2, and CCTMO-4, respectively. These results indicate that the small amount substitution of Mn^{4+} for Ti^{4+} does not change the cubic perovskite but causes a small decrease in lattice parameter as the ionic radius of Mn^{4+} is smaller than that of Ti^{4+}. To clearly indicate the lattice change, inset (d) shows the enlarged view of the (220) peak, from which we can see that the peak shifts to higher two theta values with increasing doping level. This fact demonstrates that the doping leads to the reduction in lattice parameter.

The insets (a)-(d) of Fig. 1 show the SEM images of ceramic surfaces for the pure and doped samples. The samples show dense and uniform microstructure. The relative density of all samples is more than 90 % of the theoretical value. Although the density is not high enough for electroceramics, previous reports indicate that the density has no obvious influence on the dielectric properties [28–30]. It can be seen that Mn doping is beneficial for grain growth. The average grain size was found to be around 6–8, 7–9, and 11–13 μm for CCTO, CCTMO-2, and CCTMO-4, respectively.

3.2 Dielectric properties of the three samples

Figure 2 shows the comparison of the temperature dependences of the real part of the complex permittivity, $\varepsilon'(T)$, and the dielectric loss tangent, $\tan\delta(T)$, for the three samples recorded at 300 Hz, 2 kHz, 10 kHz, 100 kHz, and 1 MHz. In general, three temperature regions can be classified (I, II, and III, as indicated in Fig. 2). It's clearly seen that a dielectric plateau exists in all samples in the temperature region I (93–300 K). The values of the dielectric plateau were obtained to be 1.0×10^4, 3.0×10^3, and 1.0×10^2 for CCTO, CCTMO-2, and CCTMO-4, respectively. The plateau for samples CCTO and CCTMO-2 was found to be followed by a rapid decrease in $\varepsilon'(T)$ at the lowest temperatures accompanied by a peak in the corresponding curve of $\tan\delta(T)$. This fact indicates that a thermally activated relaxation (termed as R1 hereafter) exists in CCTO and CCTMO-2 samples. This relaxation is the characteristic relaxation leading to the CDC behavior for CCTO. However, the plateau for the heavily doped sample CCTMO-4 develops to be a frequency-independent decline. This is the

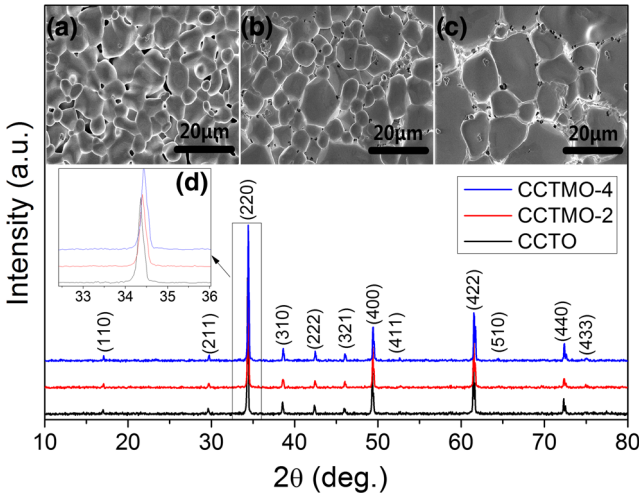

Fig. 1 XRD patens of CCTO, CCTMO-2, and CCTMO-4 ceramics. Inset shows the SEM micrographs of (**a**) CCTO, (**b**) CCTMO-2, (**c**) CCTMO-4, and (**d**) the enlarged view of the (220) reflection peaks

typical feature for incipient ferroelectric behavior and can be ascribed to the incipient ferroelectricity as reported by Li and coauthors [31]. This behavior is characterized by increasing dielectric permittivity on cooling due to the softening of the lowest frequency polar optical phonon. It is worth noting that the position of R1 in CCTMO-2 keeps almost the same as that of the pure sample. This fact indicates that Mn-doping has no obvious influence on the position of R1. However, no relaxation peaks were found in CCTMO-4 in the dielectric loss tangent curves in the temperature region I. The curves behave as frequency-independent decline in the temperature below 150 K and drastically increase in the range of 150–300 K. This is because that the incipient ferroelectric behavior is going to be replaced by the relaxation behavior due to hoping motion of oxygen vacancies, which will contribute to both conductivity and dielectric permittivity. The absence of R1 in CCTMO-4 strongly implies that the characteristic relaxation disappears rather than moving to higher temperatures.

In the temperature region II (300–600 K), two stepwise increases (SIs) in dielectric constant in CCTO can be seen. The first SI is accompanied by a set of humps in the corresponding curves of tan $\delta(T)$ spectra. The position of the hump shifts to high frequency with increasing temperature, indicating that the SI presents another thermally activated dielectric relaxation in the temperature range around room temperature. This relaxation was designated as R2. R2 can be observed in Mn-doped samples and the humps develop to be well defined peaks with their positions shifting to lower temperatures. The second SI, however, leads to a dielectric anomaly, i.e., a dielectric peak in $\varepsilon'(T)$. The low-temperature wing of the peak is accompanied by a set of tan $\delta(T)$ peaks. The positions of tan $\delta(T)$ peaks hardly change with increasing measuring frequency. This feature resembles the dielectric behavior caused

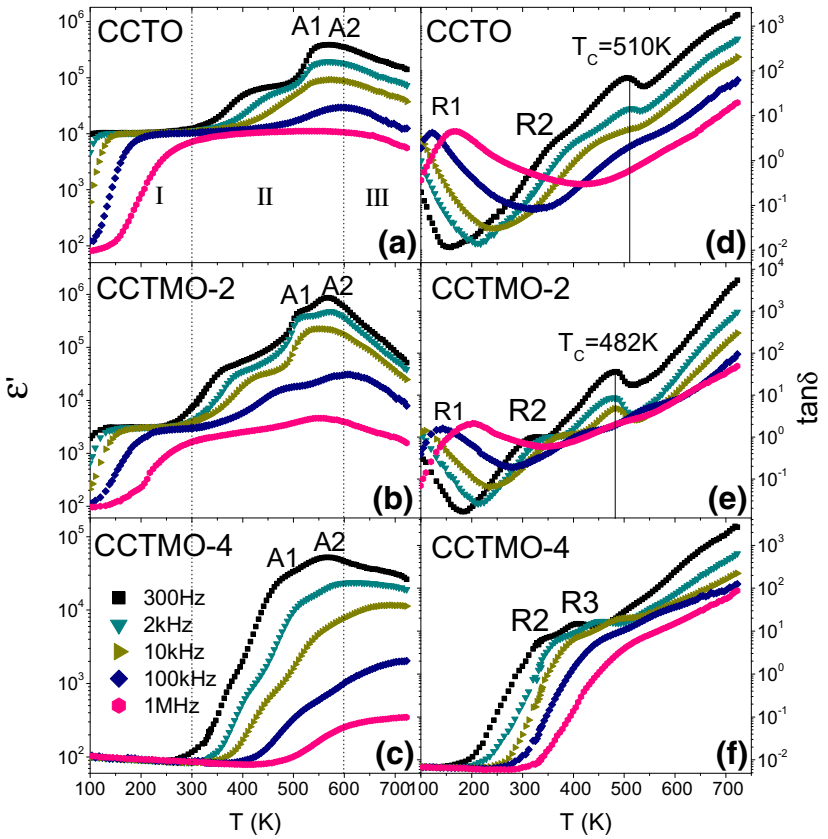

Fig. 2 Temperature dependence of ε' and tan δ for pure and Mn-doped samples: (**a**) and (**d**) CCTO, (**b**) and (**e**) CCTMO-2, and (**c**) and (**f**) CCTMO-4

by phase transition. The transition temperature T_c was found to be 510 K for CCTO. A careful examination reveals that the dielectric anomaly is composed of two peaks. They are named as A1 and A2 in the order of ascending temperature, hereafter. In CCTMO-2 the A1 and A2 peaks can be distinctly identified and the two peaks shift to lower temperatures when compared with the pure sample. The phase transition temperature was found to be 482 K. Whiles in CCTMO-4 A1 and A2 peaks further shift to lower temperatures. To our surprise, instead of the phase-transition-like peaks in $\tan\delta(T)$, a set of relaxation-like peaks (R3) were found. We shall come back to this relaxation-like feature below.

In temperature region III (600–723 K), $\varepsilon'(T)$ curves for all samples were found to monotonically decrease with increasing temperature. The curves of $\tan\delta(T)$ almost exponentially increase with temperature. This feature indicates that the conductivity contribution may dominate the dielectric properties in this region.

Since the relaxation parameter analysis is favorable for better understanding the mechanisms of the observed relations, we, therefore, focus on the calculation of the relaxation parameters for each relaxation. The dielectric peaks of R1 in the samples of CCTO and CCTMO-2, R2 and R3 in the sample of CCTMO-4 are well developed in the $\tan\delta(T)$ spectra measured with high frequencies. According to the peak position (T_p) and the measuring frequency (f), the relaxation parameters can be obtained in terms of the Arrhenius relation

$$f = f_0 \exp\left(-E_a/k_B T_p\right) \quad (1)$$

where f_0 is the pre-exponential factor, E_a is the activation energy for the relaxation, and k_B is the Boltzmann constant. Figure 3 presents the Arrhenius plots for R1, R2 and R3 observed in the three samples. The values of the activation energy and pre-exponential factor deduced from linear fittings were listed in Table 1. The activation energy value 0.096 eV of R1 is consistent with the value ~ 100 meV reported in literature [32–34]. On the other hand, the activation energy values of R2 (0.58 eV in CCTMO-2 and 0.65 eV in CCTMO-4) and R3 (0.68 eV) are also consistent with the reported value about 0.60 eV [23, 32].

To further obtain detailed information about these relaxations, the activation energy was also deduced from the frequency dependence of the electric modulus M^*, which is defined as $M^* = M' + jM'' = 1/\varepsilon^*$. It shares the same dielectric mechanism with ε^* but greatly lessens the background and becomes a "good" dielectric function in revealing the background-merged relaxation [35]. Fig. 4 displays the spectroscopic plots of the imaginary part of the electric modulus for the three samples at temperatures varying from 173 to 473 K with a step of 20 K. A notable modulus peak was observed in the high frequency range which can be identified to be R1. The insets display the enlarged part of the dashed

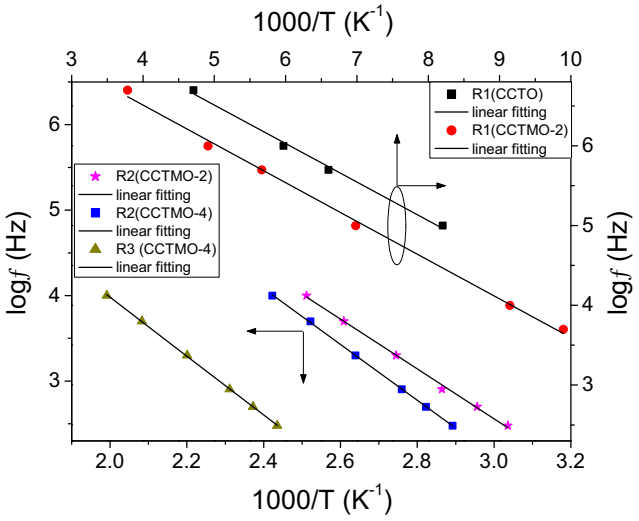

Fig. 3 The Arrhenius plots for R1, R2, and R3

rectangle area in Fig. 4(a) and (b). From which another notable peak corresponding to R2 can be seen in a wide frequency range. It is worthy of noting that the peak intensity of R1 is observed to decrease with the increasing of Mn doping level and finally vanished as the level rises to 4 at.% as shown in Fig. 4(c). On the contrary, the intensity of R2 increases with the increasing of Mn doping level and in sample CCTM-4, only R2 can be observed. These results indicate that both R1 and R2 are affected by the Mn doping.

In order to describe the relaxations and dielectric anomalies clearly, we discuss them separately in the following parts. We first focus on the characteristic relaxation observed in the temperature region I.

3.3 Dielectric relaxation in the temperature region I

The small activation energy E_a = 0.096 eV for R1 is comparable with the typical activation energy of 0.1 eV for the localized electrons hopping between multivalent Ti^{3+} and Ti^{4+} ions [17, 36]. This leads us to suppose that R1 might be concerned with polar arrangement of electrons on the mixed valence Ti^{3+}/Ti^{4+} in CCTO ceramic. It was proposed that the existence of Ti^{3+} in the sintered CCTO ceramics was either caused by oxygen loss during the high-temperature sintering process [8] or nonstoichiometry [37]. Electrons released by oxygen vacancies will be captured by Ti^{4+} to generate Ti^{3+} in the form of $Ti^{4+} + e \leftrightarrow Ti^{3+}$. Polaron relaxation occurs due to the electron hopping between Ti^{3+} and Ti^{4+} states and the electrons actually act as polarons. A characteristic feature for the polaron relaxation is that the Arrhenius plot would be deviation from the linear relationship [38]. This feature is confirmed taking CCTMO-2 as an illustration by the Arrhenius plots with the data obtained either from $M''(f)$ or from $\varepsilon''(f)$ or $\tan\delta(f)$. The deviation leads to two Arrhenius segments, as shown in Fig. 5. From these plots, the values of

Table 1 Relaxation parameters for R1, R2, and R3 found in the temperature dependence of loss tangent for CCTO, CCTMO-2, and CCTMO-4

Sample	R1		R2		R3	
	E_a (eV)	f_0 (Hz)	E_a (eV)	f_0 (Hz)	E_a (eV)	f_0 (Hz)
CCTO	0.096	2.6×10^{8}	—	—	—	—
CCTMO-2	0.096	1.4×10^{9}	0.58	9.8×10^{11}	—	—
CCTMO-4	—	—	0.65	6.4×10^{10}	0.68	8.9×10^{10}

activation energy for the low- and high-T segments are deduced to be around 80 meV and 0.11 eV, respectively. In the polaronic scenario, the hopping for localized carriers in the high-temperature range is a nearest-neighbor hopping process, which obeys the Arrhenius-like law as described by Eq. 1. Mott first pointed out that the most frequent hopping process in the low temperature range would be a variable-range-hopping process (VRH) instead of the nearest-neighbor hopping process [39]. The VRH follows the relation

$$f = f_0 \exp\left[-(T_0/T_p)^{1/4}\right] \quad (2)$$

where f_0 is the eigenfrequency and T_0 is a constant related to the activation energy. In the low-temperature range, the carriers are in a strictly localized state, then Mott's VRH sets in, leading to the distinct deviation for the Arrhenius behavior [38]. This VRH behavior in CCTO had been firstly confirmed by Zhang at el [8]. In our present sample, the VRH relation truly gives a very good straight line as shown in Fig. 5 with the top-right ordinate, which yields $f_0 = 4.73\times10^{16}$ Hz and $T_0 = 7.33\times10^{7}$ K. These values agree well with those reported in Refs. 8 and 35, giving concrete evidence for the polaronic nature of R1.

To further corroborate the polaronic nature of R1, we resort to the dielectric functions of loss tangent and electric modulus. The polaron relaxation is known to be described by Debye's theory [40]. Thus, the loss tangent and electric modulus will attain their maxima of $(\tan\delta)_{max} = (\varepsilon_s - \varepsilon_\infty)/2\sqrt{\varepsilon_s\varepsilon_\infty}$ and $(M'')_{max} = (\varepsilon_s - \varepsilon_\infty)/2\varepsilon_s\varepsilon_\infty$ at the frequency of $f_{\tan\delta} = \sqrt{\varepsilon_s/\varepsilon_\infty}/2\pi\tau$ and $f_{M''} = (\varepsilon_s/\varepsilon_\infty)/2\pi\tau$, respectively. Where ε_s and ε_∞ are the static and high-frequency dielectric constants, and τ is the relaxation time which is proportional to $\exp(-Q/k_BT)$, Q is the polaron hopping energy. The polaronic scenario predicates that the peak positions and intensities in the spectroscopic

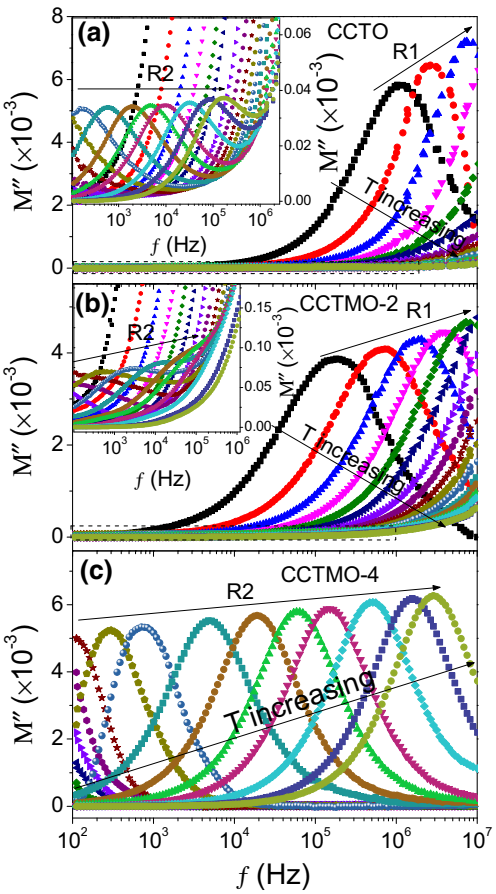

Fig. 4 Frequency dependence of M'' at temperatures from 113 to 473 K with an interval 20 K for three samples: (**a**) CCTO, (**b**) CCTMO-2, and (**c**) CCTMO-4

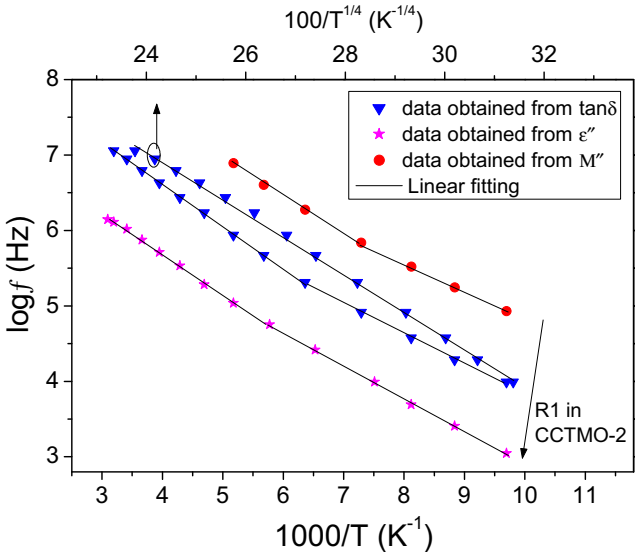

Fig. 5 The Arrhenius plot (*left and bottom axes*) of R1 found in CCTMO-2 with the date obtained form tan δ, ε'', and M''. The VRH plot (*left and top axes*) of R1 with the same data obtained form tan δ. The solid lines are linear fitting results

plots of loss tangent ($f_{\tan\delta}$, $(\tan\delta)_{max}$) and electric modulus (f_M, $(M'')_{max}$) obey the following relations

$$(f_{\tan\delta})^2/f_{M''} \infty \exp(-W_H/k_B T) \quad (3)$$

$$T(\tan)^2{}_{max}/M'' \infty \exp(-E_g/2k_B T) \quad (4)$$

where W_H and E_g are the hopping and formation energy of a polaron, respectively [41]. Two linear relations should be observed for the plots of $\log((f_{\tan\delta})^2/f_M)$ vs $1/T$ and $\log(T(\tan\delta)^2{}_{max}/M'')$ vs $1/T$. The frequency dependences of $\tan\delta(f)$ and $M''(f)$ for CCTO at several temperatures are presented in Figs. 6(a) and 4(a), respectively. From these figures, the maxima of $(\tan\delta)_{max}$ and $(M'')_{max}$ and their corresponding frequencies of $f_{\tan\delta}$ and $f_{M''}$ can be easily deduced. Figure 6(b) displays the Arrhenius plots according to Eqs. (3) and (4). Two perfect straight lines were obtained as expected, from which, W_H and $E_g/2$ are obtained to be 0.09 and 0.002 eV, respectively. For a small polaron, the activation energy for the conduction equals $E_{con} = W_H + E_g/2$ [41]. The sum of W_H and $E_g/2$ yields 0.092 eV, which is very close to the relaxation activation energy for R1 (0.089 eV). This result is in line with the polaron model as the hopping process of small polaron not only yields bulk conduction but also gives rise to dielectric relaxation with both aspects showing close values of activation energy. This finding substantially confirms the polaronic nature of R1.

The key issue is why Mn doping can effectively suppress the CDC behavior? A heuristic hint to answer this question is that the ratio of the polyvalent ions is critical for the CDC behavior [39]. Experimental evidences on Fe-based perovskites have showed that when the ratio of Fe^{2+}/Fe^{3+} is around 1:1, it is favorable for the CDC behavior [11]; when the ratio is far from 1:1 (e.g., 1:3, 1:4), it is harmful for the behavior [42, 43]. To test this point, we perform XPS measurements. Figure 7(a, b), and, (c) show the XPS spectra of Ti $2p_{3/2}$ region of CCTO, CCTMO-2, and CCTMO-4, respectively. The Ti $2p_{3/2}$ peak can be separated into two distinctive peaks by

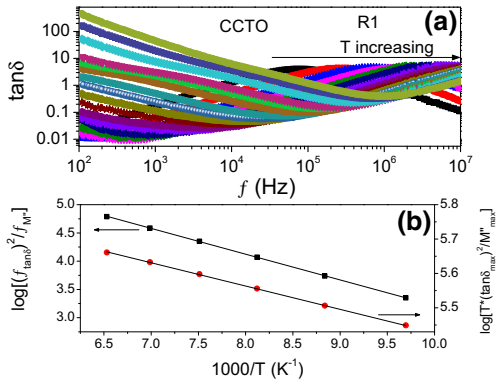

Fig. 6 **a** Frequency dependence of tan δ for CCTO at temperatures from 113 to 473 K with an interval 20 K. **b** The plots of $\log((f_{\tan\delta})^2/f_M)$ vs $1/T$ (*left*) and $\log(T(\tan\delta)^2{}_{max}/M'')$ vs $1/T$ (*right*). The solid lines are linear fitting results

Gaussian–Lorentzian curve fitting, which indicates the coexistence of Ti^{3+} (457.8 eV) and Ti^{4+} (458.4 eV) states. According to the peak area, the ratio of Ti^{3+}/Ti^{4+} was found to be 0.935, 0.8825, and 0.623 for CCTO, CCTMO-2, and CCTMO-4, respectively. It is seen that Mn-doping can effectively decreases creases the Ti^{3+}/Ti^{4+} ratio. It is seen that the ratio of the pure sample is around 1:1, which is slightly decreased in the 2 at. % Mn-doped sample. Therefore, CDC behavior can be observed in both samples but with somewhat reduction in magnitude in the 2 at. % Mn-doped sample (see Fig. 2). Further increasing the Mn doping level to 4 at. % produces a remarkable decrease in the Ti^{3+}/Ti^{4+} ratio, resulting in the disappearance of the CDC behavior in CCTMO-4 sample. This result indicates that the effect of Mn-doping is to suppress the Ti^{3+}/Ti^{4+} ratio. This effect can be understood based on the fact that electrons released by oxygen vacancies will be captured by Ti^{4+} to generate Ti^{3+} in the form of $Ti^{4+} + e \leftrightarrow Ti^{3+}$. Dipolar effect occurs due to the electron hopping between Ti^{3+} and Ti^{4+} states and the electrons actually act as polarons. When Mn^{4+} ions occupy the sites of Ti^{4+}, the electrons are much more easily captured by Mn^{4+} due to the ionic radius of Mn^{4+} (0.54 Å) is smaller than the ionic radius of Ti^{4+} (0.64 Å). Therefore, less Ti^{3+} ions were formed.

The above finding seems to demonstrate that the characteristic relaxation of CCTO (R1) is related to the hopping of electrons between Ti^{3+} and Ti^{4+} ions. However, caution should be made when come to this conclusion, because there are two polyvalent cations (Cu and Ti) in CCTO. A low Ti^{3+}/Ti^{4+} ratio of 0.45 was found in $CaCu_3(Ti_{0.9}Sn_{0.1})_4O_{12}$, but the room temperature dielectric permittivity values of the sample were very high (> 10^4) over a frequency from 10^2 to 10^5 Hz [44]. This fact indicates that the ratio of Ti^{3+}/Ti^{4+} alone is insufficient to describe the CDC behavior in CCTO. Other sources of intrinsic factor, such as the presence of Cu + and Cu^{3+} or other, may also result in the colossal dielectric response in Mn-doped CCTO [44, 45]. To investigate the oxidation states of Cu, Fig. 7d, e and f display the XPS spectra of Cu $2p_{3/2}$ region of CCTO, CCTMO-2, and CCTMO-4, respectively. By using Gaussian–Lorentzian fitting, the $2p_{3/2}$ peak for Cu can be divided into two peaks: the first peak locating at around 933.67 eV corresponds to Cu^{2+} [45]; the second peak appearing at around 935.32 eV is related to Cu^{3+} [46]. It is surprised that no Cu^{1+} signal is detected as this signal have been extensively reported in literature [44–46]. The ratio of Cu^{3+}/Cu^{2+} was found to be 1.460, 0.681, and 0.676 for CCTO, CCTMO-2, and CCTMO-4, respectively. The presence of Cu^{3+} indicates that Cu vacancies appear at grain-boundary layers [47, 48]. The Cu-poor as well as Ca- or Ti-rich at the outmost layers of grains were considered to be the origin of the internal barrier-layer (IBL) structure [49]. Obviously, Mn-doping greatly suppresses the ratio of Cu^{3+}/Cu^{2+}. In other words, the doping is harmful for the formation of the IBL structure. According to the internal barrier-layer

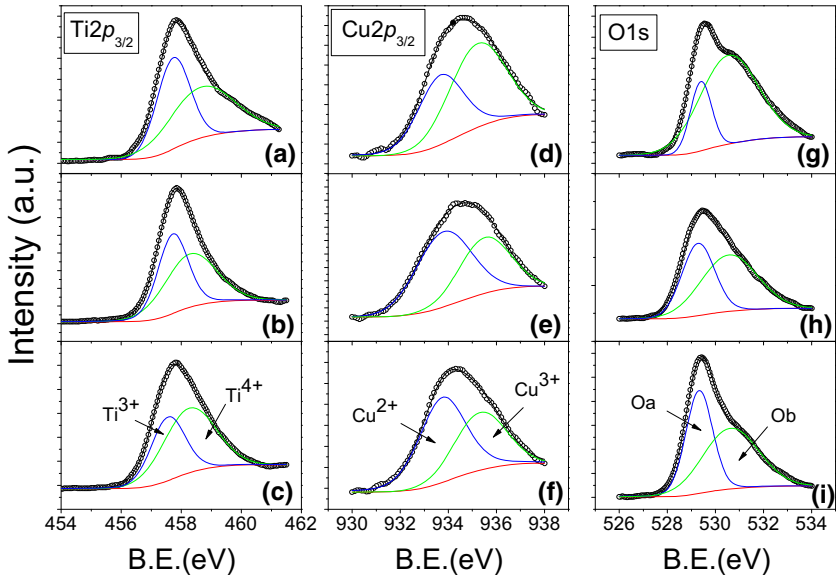

Fig. 7 XPS spectra of Ti-2p (**a**–**c**), Cu-2p (**d**–**f**), and O-1 s (**g**–**i**) for CCTO (*top panels*), CCTMO-2 (*middle panels*), and CCTMO-4 (*bottom panels*)

capacitance model [4], Mn-doping is unfavorable for the CDC behavior.

Based on the polaron scenario, the relaxation R1 depends not only on the ratio of Ti^{3+}/Ti^{4+}, but also on the concentration of electrons. Mn-doping can effectively change the ratios of polyvalent ions, it can be expected to change the concentration of oxygen vacancies for sake of charge compensation. To clarify this point, Fig. 7(g, h and i) compare the O1s XPS spectra of CCTO, CCTMO-2, and CCTMO-4, respectively. The spectra can be fitted with two Gaussian peaks which are denoted as Oa and Ob peaks. The Oa peak with a low binding energy of 529.281–529.398 eV is ascribed to the O^{2-} in the CCTO lattice sites, while the Ob peak showing a high binding energy of 530.560–530.630 eV is related to the oxygen vacancies [50]. The area of Ob/Oa was calculated to be 3.533, 1.326, and 1.175 for CCTO, CCTMO-2, and CCTMO-4, respectively. This finding indicates that Mn-doping notably decreases the concentration of oxygen vacancies, which in turn, decreases the concentration of electrons. This factor is also adverse to the CDC behavior.

In summary, the characteristic relaxation of CCTO (R1) is a polaron relaxation caused by the hopping motions of electrons between Ti^{3+} and Ti^{4+} ions. Mn-doping leads to the notable decreases in the ratios of Ti^{3+}/Ti^{4+} and Cu^{3+}/Cu^{2+} and the concentration of oxygen vacancies. All of these effects have negative impacts on the CDC behavior.

3.4 Dielectric relaxations and anomalies in the temperature region II

Figure 8 displays the Arrhenius plots of R2 with data obtained from $M''(f)$ for the three samples. The activation energy and pre-exponential factor for CCTO, CCTMO-2, CCTMO-4 were calculated to be 0.55, 0.58, 0.61 eV, and 1.2×10^{11}, 2.1×10^{11}, 1.7×10^{11} Hz, respectively. R2 can be ruled out to be a polaron relation due to electron hopping between $Mn^{3+}$and Mn^{4+} ions, because the activation value is much larger than ~0.40 eV required for such relaxation [27]. These values are consistent with those obtained from $\tan\delta(T)$ and agree well with values of $E_a = 0.59$ eV and $f_0 = 1/5.619 \times 10^{-12} = 1.78 \times 10^{11}$ Hz for the Maxwell-Wagner (MW) relaxation [51]. This fact strongly implies that R2 might be a MW relaxation.

In order to gain more information about the relaxation R2, the frequency dependence of the real part of the complex permittivity, $\varepsilon'(f)$, for the three samples was measured at temperatures varying from 173 to 473 K with a step of 20 K. As shown in Fig. 9(a), the CDC behavior of CCTO results from two thermally activated relaxations. For a thermally activated relaxation, the high (low)-frequency relaxation in the frequency spectra corresponds to the low (high)-temperature relaxation in the temperature spectra. So, the relaxation occurring in the high-frequency region (region I, as indicated in the figure) is corresponding to R1, while the relaxation appearing

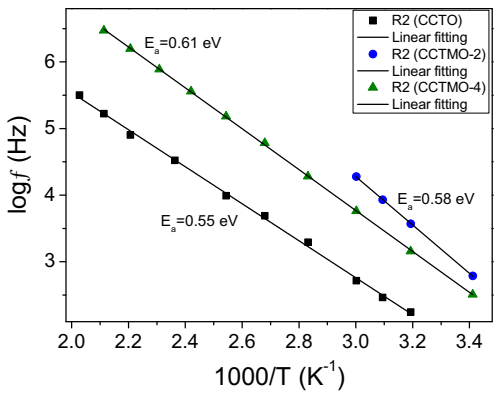

Fig. 8 Arrhenius plots of R2 for CCTO, CCTMO-2, and CCTMO-4. The solid lines are linear fitting results

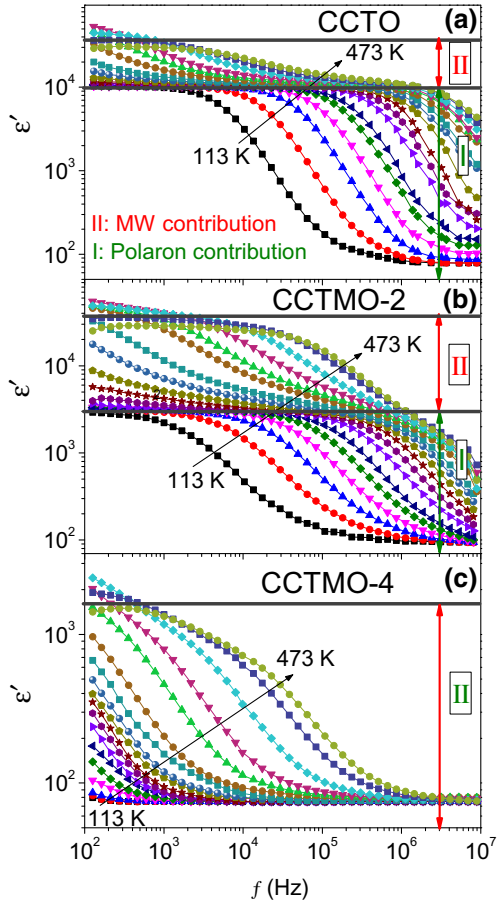

Fig. 9 Frequency dependence of ε' for (**a**) CCTO, (**b**) CCTMO-2, and (**c**) CCTMO-4 in the temperature range of 113–473 K with $\Delta T = 20$ K

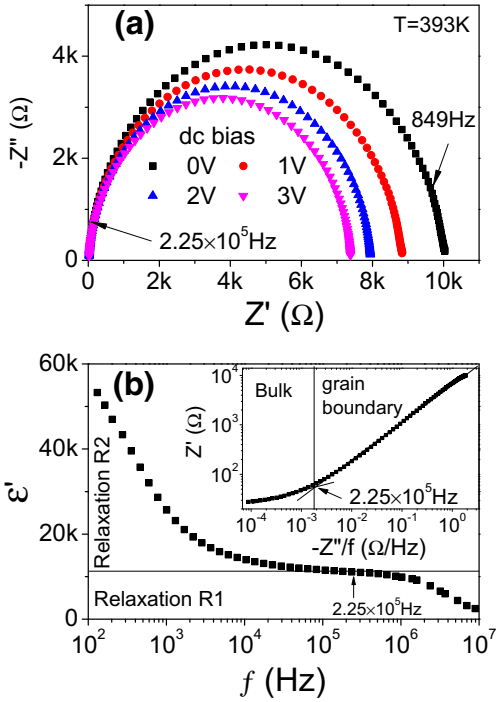

Fig. 10 **a** Nyquist plot of the CCTO measured at 393 K under different dc biases. **b** Frequency dependence of dielectric constant for CCTO at 393 K. The inset shows an alternative representation of Z' vs Z''/f for the impedance data under zero dc bias presented in Fig. 10(a)

afterward (region II) is corresponding to R2. The value of the dielectric plateau in region I is found to be notably decreased in CCTMO-2 sample (please note the logarithmic scale of $\varepsilon'(f)$) and disappears completely in CCTMO-4 sample. These results are consistent with those of observed in Fig. 2, and confirm that the multi-relaxation mechanism, i.e., the coupling of a polaron relaxation and a MW relaxation is responsible for the CDC behavior [52]. In this scenario, R2 should be a MW relaxation.

The MW nature for R2 can be convinced by further impedance analysis. We take the data of CCTO recorded at 393 K as an example. Figure 10(a) displays the Nyquist plot measured under different dc biases by illustrating $-Z''$ versus Z', where Z' and Z'' are the real and imaginary parts of the complex impedance Z^*. The Nyquist plot displays a semicircle. It is clearly seen that the low-frequency part of the semicircle can be remarkably depressed by the dc bias, whereas the high-frequency part is almost bias-independent. This fact indicates the Nyquist plot contains overlapped semicircles with the low-frequency part corresponding to the interfacial response and the high-frequency one corresponding to the bulk response [53]. To separate the different contributions, the representation of Z' versus $-Z''/f$ is known as an effective method to distinguish the dielectric responses from the contacts, grain boundaries, and bulk grains even with relatively small differences [54]. In the inset of Fig. 10(b), the data without dc bias were replotted in the representation of Z' versus $-Z''/f$. Two linear segments with a boundary frequency $f = 2.25 \times 10^5$ Hz can be identified. The low- and high-frequency regions can be ascribed to the dielectric responses from the grain-boundary and bulk, respectively. The boundary frequency was also indicated in the Nyquist plot, which clearly shows that the grain-boundary response contributes the main body of the Nyquist plot.

The spectroscopic plot of $\varepsilon'(f)$ recorded at 393 K in Fig. 9(a) was replotted in the main panel of Fig. 10(b). The boundary frequency was also indicated in this figure. From this figure, we can see that the boundary frequency distinctly separates R1 and R2, both behave as a rapid decrease in $\varepsilon'(f)$). Therefore, relaxation R2 is a MW relaxation caused by grain boundary.

Based on the above results, let's come back to Fig. 9. It is obvious that the CDC behavior found in CCTO and CCTMO-2 results from both polaron and MW contributions. In CCTO, the polaron and MW contributions are 1.0×10^4 and 2.6×10^4, respectively. In CCTMO-2, these values are found to be 3.0×10^3 and 3.4×10^4. While in CCTMO-4, only the MW contribution of $\sim 1.6 \times 10^3$ is found. These findings demonstrate (1) the multi-relaxation mechanism for the CDC behavior in CCTO systems and (2) the CDC behavior is mainly contributed by the MW contribution. Meanwhile, Mn-

doping effectively suppresses the polaron contribution; but enhances the MW contribution at lower doping level and destroys the MW contribution at higher doping level. The reason for the former case is that Mn-doping decreases the ratio of Ti^{3+}/Ti^{4+}. Whereas for the latter case, the changes of both Cu^{3+}/Cu^{2+} ratio and oxygen vacancies concentration may affect the IBL structure at the grain boundaries.

We now turn our attention to R3. In Fig. 9, one notes that the dielectric constant below about 1 kHz for all samples first increases and then decreases with the temperature increasing. This result demonstrates that the free-carrier effect at high enough temperatures. Since the free carriers have no contribution to $\varepsilon'(T)$, when more and more relaxing species become free ones, a great reduction in $\varepsilon'(f)$ and even a negative-capacitance effect leading to the appearance of a dielectric anomaly. The anomaly initially occurs at low frequencies and gradually moves to high frequencies [55]. To our surprise, the spectroscopic plots of $\varepsilon'(f)$ well describe the evolution of R1 and R2, but without no signals of R3 even in the temperature range where R3 can be clearly identified in $\varepsilon'(T)$. The absence of R3 in the frequency spectra illustrates that it is a non-relaxational process, because for the non-relaxational peak in the temperature spectra there is no correspondence in the frequency spectra [56]. The non-relaxational process is widely reported to be related to a phase transition process [55, 56]. Therefore, R3 is virtually associated with the phase-transition-like dielectric anomaly observed in CCTO and CCTMO-2 samples.

In the temperature between 300 and 600 K, a relaxor-like dielectric anomaly was frequently reported in CCTO by different authors [19, 57–62]. Our recent results demonstrated that the anomaly in CCTO results from the co-contribution from dipolar and MW relaxations caused by oxygen vacancies [51]. The anomaly A1 in the present samples was accompanied by a set of phase-transition-like peaks in $\tan\delta(T)$ curves. This feature indicates that A1 does not belong to the relaxor-like anomaly. Previous work showed that the phase-transition-like anomaly is neither symmetry breaking nor endothermic/exothermic. It is related to the redistribution of oxygen vacancies from the static disordered state to the dynamic disorder state [56, 63]. This kind of phase transition is virtually related to the ionic conduction mechanism changing from the thermally activated behavior in the lower temperature range to the thermally assisted behavior in the higher temperature range [64]. The latter is a collective behavior, therein the lattice distortions induced by two neighboring oxygen vacancies are overlapped. Thus, the transition depends not only on the concentration of oxygen vacancies but also on the doping level. A small amount of the doping level can notably enhance this transition, but excessive doping would destroy this transition [57]. As shown in Fig. 2(b) and (c), with the amount of Mn doping level increase, the transition is first enhanced in CCTMO-2 and then decreased in CCTMO-4. Mn-doping may favor the thermally assisted mechanism of conduction, therefore, enhancing the transition. On the other hand, the appearance of oxygen vacancies is the requirement of electric neutrality. The side effect induced by a vacancy is that the adjacent ions around the vacancy will move inward yielding lattice distortion. Mn-doping further enhances the distortion as revealed by the XRD analysis (see Fig. 1). This is energetically detrimental to the formation of oxygen vacancies as already confirmed by the XPS result. Therefore, excessive doping is unfavorable for the transition. Based on the above discussion, A1 can be reasonably ascribed to the distribution state transition for oxygen vacancies.

As to the dielectric anomaly A2, it is seen that A2 appears in the temperature range where $\tan\delta(T)$ sharply increases with temperature. It is well-known that there are two sources contributing to the dielectric permittivity: dielectric polarization and conductivity. Strictly localized carriers give rise to polarization effect under an applied electric field. This effect dominates the dielectric properties in the low temperature range. In the medium temperature range, the carriers become weakly localized, they can contribute to both conductivity and polarization via hoping motion. The dielectric properties in this range can be described by the famous law of universal dielectric response [65]. In high enough temperature range, the carriers becomes free carriers giving rise to dc conductivity, which has contribution to the imaginary part of the permittivity depending on the concentration of the free carriers and frequently following a thermally activated behavior. Hence, this kind of contribution to the imaginary (real) part of the permittivity increases (decreases) significantly with increasing temperature. It is, therefore, expected that there exists a critical temperature, beyond which the conductivity contribution surpasses the polarization contribution and dominates the behavior of the dielectric loss in the high temperature range. Meanwhile, this makes the ceramic sample highly leaky. Li et al. pointed out that, in this case, the inductive effect of the measuring system becomes evident [66]. This will lead to negative capacitance effect, giving rise to a dielectric anomaly in $\varepsilon'(T)$. The negative capacitance is confirmed as shown in Fig. 11 by measuring the temperature dependence of the capacitance to higher temperatures. Therefore, the anomaly A2 is an artificial effect caused by negative capacitance.

3.5 Dielectric behavior in the temperature region III

As aforementioned, the conductivity contribution may dominate the dielectric properties in this region. The contribution from dc conductivity takes the form

$$\varepsilon''(\omega, T) = \sigma_{dc}/\omega\varepsilon_0 = \sigma_0 \exp(-E_{con}/k_B T)/\omega\varepsilon_0 \quad (5)$$

where σ_{dc} is the dc conductivity, ε_0 is the vacuum permittivity, σ_0 is the pre-exponential factor, and E_{con} is the activation

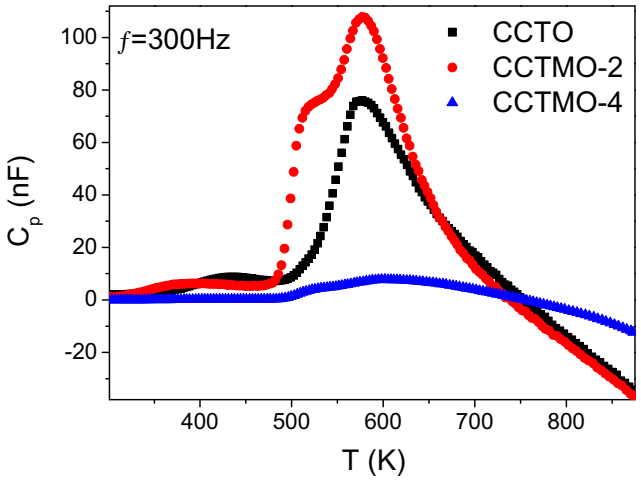

Fig. 11 Temperature dependence of capacitance recorded at 300 Hz for CCTO, CCTMO-2, and CCTMO-4 measured to higher temperatures up to 873 K

energy for conductivity. Thus, a linear relationship will be obtained if $\log \varepsilon''$ is plotted as a function of the reciprocal of temperature. This inference is convinced in Fig. 12, therein the plots of $\log \varepsilon''$ vs $1000/T$ at the selected frequencies for all samples show linear lines in the high-temperature range. The slopes of these lines yield the values of E_{con}, which were calculated to be 0.53, 0.54, and 0.61 eV for CCTO, CCTMO-2, and CCTMO-4, respectively. Hence, the dielectric behavior in the temperature region III is mainly controlled by the conductivity.

4 Conclusions

Pure, and 2, and 4 at.% Mn-doped CCTO ceramics were prepared using the conventional solid-state reaction method.

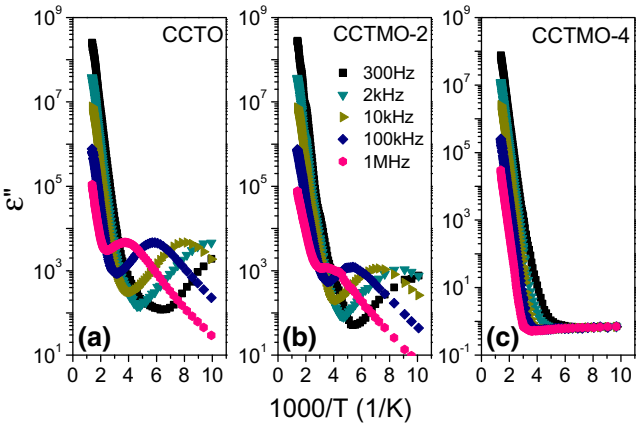

Fig. 12 The imaginary part of the complex dielectric permittivity was plotted as a function of $1/T$ for (**a**) CCTO, (**b**) CCTMO-2, and (**c**) CCTMO-4

The dielectric properties of samples were investigated as functions of temperature (93–723 K) and frequency ranging from 100 Hz to 10 MHz. Two dielectric relaxations and two anomalies were found. Our results reveal that:

1. The low-temperature relaxation appearing below 200 K is a polaron relaxation due to electrons hoping between Ti^{3+} and Ti^{4+} states. The high-temperature relaxation appearing around room temperature is a MW relaxation caused by grain boundary response.
2. The effects of Mn doping were found to remarkably decrease the ratios of Ti^{3+}/Ti^{4+} and Cu^{3+}/Cu^{2+}, and the concentration of oxygen vacancies. Therefore, Mn doping is harmful for the CDC behavior.
3. Our results confirm the multi-relaxation mechanism for the CDC behavior in CCTO and the CDC behavior is mainly dominated by the MW contribution.
4. The high-temperature anomaly was caused by the redistribution for oxygen vacancies from the static disordered state to the dynamic disorder state. Whereas the high-temperature anomaly was caused by the negative capacitive effect.

Acknowledgments The authors thank financial support from National Natural Science Foundation of China (Grant Nos 11404002, 11404003, and 51402001) and Co-operative Innovation Research Center for Weak Signal-Detecting Materials and Devices Integration of Anhui University (Grant No 01001795).

References

1. M.A. Subramanian, D. Li, N. Duan, B.A. Reisner, A.W. Sleight, High dielectric constant in $ACu_3Ti_4O_{12}$ and $ACu_3Ti_3FeO_{12}$ phases. J. Solid State Chem. **151**, 323–325 (2000)
2. M.H. Cohen, J.B. Neaton, L.X. He, D. Vanderbilt, Extrinsic models for the dielectric response of $CaCu_3Ti_4O_{12}$. J. Appl. Phys. **94**, 3299–3306 (2003)
3. P. Lunkenheimer, R. Fichtl, S.G. Ebbinghaus, A. Loidl, Nonintrinsic origin of the colossal dielectric constants in $CaCu_3Ti_4O_{12}$. Phys. Rev. B **70**, 172102 (2004)
4. D.C. Sinclair, T.B. Adams, F.D. Morrison, A.R. West, $CaCu_3Ti_4O_{12}$: one-step internal barrier layer capacitor. Appl. Phys. Lett. **80**, 2153–2155 (2002)
5. T.B. Adams, D.C. Sinclair, A.R. West, Giant barrier layer capacitance effects in $CaCu_3Ti_4O_{12}$ ceramics. Adv. Mater. **14**, 1321–1323 (2002)
6. C.C. Homes, T. Vogt, S.M. Shapiro, S. Wakimoto, A.P. Ramirez, Optical response of high-dielectric constant perovskite-related oxide. Science **293**, 673–676 (2001)
7. A.P. Ramirez, M.A. Subramanian, M. Gardel, G. Blumberg, D. Li, T. Vogt, S.M. Shapiro, Giant dielectric constant response in a copper-titanate. Solid State Commun. **115**, 217–220 (2000)
8. L. Zhang, Z.J. Tang, Polaron relaxation and variable-range-hopping conductivity in the giant-dielectric-constant material $CaCu_3Ti_4O_{12}$. Phys. Rev. B **70**, 174306 (2004)
9. L. Ni, X.M. Chen, Dielectric relaxations and formation mechanism of giant dielectric constant step in $CaCu_3Ti_4O_{12}$ ceramics. Appl. Phys. Lett. **91**, 122905 (2007)

10. D.K. Mahato, A. Dutta, T.P. Sinha, Dielectric relaxation in double perovskite oxide, Ho_2CdTiO_6. Bull. Mater. Sci. **34**, 455–462 (2011)
11. N. Ikeda, H. Ohsumi, K. Ohwada, K. Ishii, T. Inami, K. Kakurai, Y. Murakami, K. Yoshii, S. Mori, Y. Horibe, H. Kito, Ferroelectricity from iron valence ordering in the charge-frustrated system $LuFe_2O_4$. Nature **436**, 1136–1138 (2005)
12. S.M. Ke, H.Q. Fan, H.T. Huang, Dielectric relaxation in A_2FeNbO_6 (A = Ba, Sr, and Ca) perovskite ceramics. J. Electroceram. **22**, 252–256 (2009)
13. X.G. Zheng, Y. Sakurai, Y. Okayama, T.Q. Yang, L.Y. Zhang, X. Yao, K. Nonaka, C.N. Xu, Dielectric measurement to probe electron ordering and electron-spin interaction. J. Appl. Phys. **92**, 2703–2708 (2002)
14. W.Z. Yang, M.M. Mao, X.Q. Liu, X.M. Chen, Structure and dielectric relaxation of double-perovskite La_2CuTiO_6 ceramics. J. Appl. Phys. **107**, 124102 (2010)
15. X.H. Sun, C.C. Wang, G.J. Wang, C.M. Lei, T. Li, L.N. Liu, Low-temperature relaxations associated with mixed-valent structure in Sr_2TiMnO_6. J. Am. Ceram. Soc. **96**, 513–518 (2013)
16. X.H. Sun, C.C. Wang, G.J. Wang, C.M. Lei, T. Li, L.N. Liu, Low-temperature dielectric relaxations associated with mixed-valent structure in $Na_{0.5}Bi_{0.5}Cu_3Ti_4O_{12}$. J. Am. Ceram. Soc. **96**, 1497–1503 (2013)
17. M. Magline, M.A. Subramanian, Dielectric and polarization experiments in high loss dielectrics: a word of caution. Appl. Phys. Lett. **93**, 032903 (2008)
18. B.S. Prakash, K.B.R. Varma, Effect of sintering conditions on the dielectric properties of $CaCu_3Ti_4O_{12}$ and $La_{2/3}Cu_3Ti_4O_{12}$ ceramics: a comparative study. Physica B **382**, 312–319 (2006)
19. C.C. Wang, L.W. Zhang, Oxygen-vacancy-related dielectric anomaly in $CaCu_3Ti_4O_{12}$: post-sintering annealing studies. Phys. Rev. B **74**, 024106 (2006)
20. Y.H. Lin, W. Deng, W. Xu, Y. Liu, D.L. Chen, X.L. Zhang, C.W. Nan, Abnormal dielectric behaviors in Mn-doped $CaCu_3Ti_4O_{12}$ ceramics and their response mechanism. Mater. Sci. Eng. B **177**, 1773–1776 (2012)
21. W. Kobayashi, I. Terasaki, Unusual impurity effects on the dielectric properties of $CaCu_{3-x}Mn_xTi_4O_{12}$. Physica B **329**, 771–772 (2003)
22. M. Li, A.F. Feterira, D.C. Sinclair, A.R. West, Influence of Mn doping on the semiconducting properties of $CaCu_3Ti_4O_{12}$ ceramics. Appl. Phys. Lett. **88**, 232903–232905 (2006)
23. R.K. Grubbs, E.L. Venturini, P.G. Clem, J.J. Richardson, B.A. Tuttle, G.A. Samara, Dielectric and magnetic properties of Fe- and Nb-doped $CaCu_3Ti_4O_{12}$. Phys. Rev. B **72**, 104111 (2005)
24. J.N. Cai, Y.H. Lin, B. Cheng, C.W. Nan, J.L. He, Y.J. Wu, X.M. Chen, Dielectric and nonlinear electrical behaviors observed in Mn-doped$CaCu^3Ti_4O_{12}$ ceramic. Appl. Phys. Lett. **91**, 252905 (2007)
25. C.H. Kim, Y.H. Jang, S.J. Seo, C.H. Song, J.Y. Son, Y.S. Yang, J.H. Cho, Effect of Mn doping on the temperature-dependent anomalous giant dielectric behavior of $CaCu_3Ti_4O_{12}$. Phys. Rev. B **85**, 245210 (2012)
26. P. Lunkenheimer, S. Krohns, S. Riegg, S.G. Ebbinghaus, A. Reller, A. Loidl, Colossal dielectric constants in transition-metal oxides. Eur. Phys. J. Spec. Top. **180**, 61–89 (2010)
27. J. Yang, X.J. Meng, M.R. Shen, L. Fang, J.L. Wang, T. Lin, J.L. Sun, J.H. Chu, Hopping conduction and low-frequency dielectric relaxation in 5 mol % Mn doped (Pb, Sr)TiO3 films. J. Appl. Phys. **104**, 104113 (2008)
28. Q. Zheng, H.Q. Fan, C.B. Long, Microstructures and electrical responses of pure and chromium-doped $CaCu_3Ti_4O_{12}$ ceramics. J. Alloy. Compd. **511**, 90–94 (2012)
29. Q. Zheng, H.Q. Fan, Influence of fabrication parameters on the phase formation and dielectric properties of $CaCu_3Ti_4O_{12}$ ceramics. J. Mater. Sci. Technol. **28**, 920–926 (2012)
30. H.Q. Fan, Q. Zheng, B.L. Peng, Microstructure, dielectric and pyroelectric properties of $CaCu_3Ti_4O_{12}$ ceramics fabricated by tape-casting method. Mater. Res. Bull. **48**, 3278–3283 (2013)
31. M. Li, A. Feteira, D.C. Sinclair, A.R. West, Incipient ferroelectricity and microwave dielectric response properties of $CaCu_{2.85}Mn_{0.15}Ti_4O_{12}$ ceramics. Appl. Phys. Lett. **91**, 132911 (2007)
32. J.L. Zhang, P. Zheng, C.L. Wang, M.L. Zhao, J.C. Li, J.F. Wang, Dielectric dispersion of $CaCu_3Ti_4O_{12}$ ceramics at high temperatures. Appl. Phys. Lett. **87**, 142901 (2005)
33. J.R. Li, K. Cho, N.J. Wu, Correlation between dielectric properties and sintering temperatures of polycrystalline $CaCu_3Ti_4O_{12}$. IEEE Trans. Dielectr. Electr. Insul. **11**, 534–541 (2004)
34. J.J. Liu, C.G. Duan, W.G. Yin, W.N. Mei, R.W. Smith, J.R. Hardly, Large dielectric constant and Maxwell-Wagner relaxation in $Bi_{2/3}Cu_3Ti_4O_{12}$. Phys. Rev. B **70**, 144106 (2004)
35. C.C. Wang, J. Wang, X.H. Sun, L.N. Liu, J. Zhang, J. Zheng, C. Cheng, Oxygen-vacancy-related dielectric relaxations in $Na_{0.5}K_{0.5}NbO_3$. Solid State Commun. **179**, 29–33 (2014)
36. O. Bidault, M. Maglione, M. Actis, M. Kchikech, B. Salce, Polaronic relaxation in perovskites. Phys. Rev. B **52**, 4191–4197 (1995)
37. T.B. Adams, D.C. Sinclair, A.R. West, Influence of processing conditions on the electrical properties of $CaCu_3Ti_4O_{12}$Ceramics. J. Am. Ceram. Soc. **89**, 3129–3135 (2006)
38. C.C. Wang, L.W. Zhang, Polaron relaxation related to localized charge carriers in $CaCu_3Ti_4O_{12}$. Appl. Phys. Lett. **90**, 142905 (2007)
39. N.F. Mott, E.A. Davis, *Electronic Processes in Noncrystalline Materials* (Clarendon, Oxford, 1979)
40. H. Frohlich, *Theory of Dielectrics: Dielectric Constant and Dielectric Loss* (Clarendon, Oxford, 1958)
41. E. Iguchi, K. Ueda, W.H. Jung, Conduction in $LaCoO_3$ by small-polaron hopping below room temperature. Phys. Rev. B **54**, 17431 (1996)
42. Y. Ma, X.M. Chen, Y.Q. Liu, Relaxorlike dielectric behavior and weak ferromagnetism in $YFeO_3$ ceramics. J. Appl. Phys. **103**, 12411 (2008)
43. J.L. Ye, C.C. Wang, W. Ni, X.H. Sun, Dielectric properties of $ErFeO_3$ceramics over a broad temperature range. J. Alloy. Compd. **617**, 850–854 (2014)
44. L. Ni, X.M. Chen, X.Q. Liu, Structure and modified giant dielectric response in $CaCu_3(Ti_{1-x}Sn_x)_4O_{12}$ ceramics. Mater. Chem. Phys. **124**, 982–986 (2010)
45. P. Thongbai, J. Jumpatam, B. Putasaeng, T. Yamwong, S. Maensiri, The origin of giant dielectric relaxation and electrical responses of grains and grain boundaries of W-doped $CaCu_3Ti_4O_{12}$ ceramics. J. Appl. Phys. **112**, 114115 (2012)
46. P. Thongbai, J. Jumpatam, T. Yamwong, S. Maensiri, Effects of Ta^{5+} doping on microstructure evolution, dielectric properties and electrical response in $CaCu_3Ti_4O_{12}$ ceramics. J. Eur. Ceram. Soc. **32**, 2423–2430 (2012)
47. T.T. Fang, L.T. Mei, H.F. Ho, Effects of Cu stoichiometry on the microstructures, barrier-layer structures, electrical conduction, dielectric responses, and stability of $CaCu_3Ti_4O_{12}$. Acta Mater. **54**, 2867–2875 (2006)
48. C. Wang, H.J. Zhang, P.M. He, G.H. Cao, Ti-rich and Cu-poor grain-boundary layers of $CaCu_3Ti^4O_{12}$ detected by x-ray photoelectron spectroscopy. Appl. Phys. Lett. **91**, 052910 (2007)
49. T.T. Fang, L.T. Mei, Evidence of Cu deficiency: a key point for the understanding of the mystery of the giant dielectric constant in $CaCu_3Ti_4O_{12}$. J. Am. Ceram. Soc. **90**, 638–640 (2007)
50. X.J. Xi, S.Y. Wang, W.F. Liu, H.J. Wang, F. Guo, X. Wang, J. Gao, D.J. Li, Enhanced magnetic and conductive properties of Ba and Co co- doped $BiFeO_3$ ceramics. J. Magn. Magn. Mater. **355**, 259–264 (2014)

51. C.C. Wang, M.N. Zhang, K.B. Xu, G.J. Wang, Origin of high-temperature relaxor-like behavior in $CaCu_3Ti_4O_{12}$. J. Appl. Phys. **112**, 034109 (2012)
52. G.J. Wang, C.C. Wang, S.G. Huang, C.M. Lei, X.H. Sun, T. Li, L.N. Liu, Origin of colossal dielectric behavior in double perovskite Ba_2CoNbO_6. J. Am. Ceram. Soc. **96**, 2203–2210 (2013)
53. C.C. Wang, M. He, F. Yang, J. Wen, G.Z. Liu, H.B. Lu, Enhanced tunability due to interfacial polarization in $La_{0.7}Sr_{0.3}MnO_3/BaTiO_3$ multilayers. Appl. Phys. Lett. **90**, 192904 (2007)
54. C.C.A. João, A. João, R.F. Jorge, An alternative representation of impedance spectra of ceramics. Mater. Res. Bull. **35**, 727–740 (2000)
55. L.N. Liu, C.C. Wang, C.M. Lei, T. Li, G.J. Wang, X.H. Sun, J. Wang, S.G. Huang, Y.D. Li, H. Wang, Relaxor- and phase-transition-like behaviors in ZnO single crystals at high temperatures. Appl. Phys. Lett. **102**, 112907 (2013)
56. D. Li, X.P. Wang, Q.F. Fang, J.X. Wang, C. Li, Z. Zhuang, Phase transition associated with the variation of oxygen vacancy/ion distribution in the oxide-ion conductor $La_2Mo_{2-x}W_xO_9$. Phys. Stat. Sol. (a) **204**, 2270–2278 (2007)
57. S.M. Ke, H.T. Huang, H.Q. Fan, Relaxor behavior in $CaCu_3Ti_4O_{12}$ ceramics. Appl. Phys. Lett. **89**, 182904 (2006)
58. H.T. Yu, H.X. Liu, H. Hao, L.L. Guo, C.J. Jin, Z.Y. Yu, M.H. Cao, Grain size dependence of relaxor behavior in $CaCu_3Ti_4O_{12}$ ceramics. Appl. Phys. Lett. **91**, 222911 (2007)
59. B.S. Prakash, B.R. VarmaK, Ferroelectriclike and pyroelectric behavior of $CaCu_3Ti_4O_{12}$ ceramics. Appl. Phys. Lett. **90**, 082903 (2007)
60. A. Onadera, K. Kawatani, M. Takesada, M. Oda, M. Ido, Dielectric and thermal properties of single-crystalline $CaCu_3Ti_4O_{12}$ at higher temperatures. Jpn. J. Appl. Phys. Part 1 **48**, 09KF12 (2009)
61. A. Onadera, M. Takesada, K. Kawatani, S. Hiramatsu, Dielectric properties and phase transition in $CaCu_3Ti_4O_{12}$ at high temperatures. Jpn. J. Appl. Phys. Part **1**(47), 7753–7756 (2008)
62. A. Onodera, M. Takesada, Anomalous dielectric behavior in $CaCu_3Ti_4O_{12}$ at high temperatures. Ferroelectrics **379**, 15–21 (2009)
63. Q.F. Fang, Z. Zhuang, X.P. Wang, D. Li, J.X. Wang, Phase transition and oxygen ion diffusion in $(La_{1-x}Ln_x)_2Mo_2O_9$ (Ln = Nd, Gd, x = 0.05-0.25) using dielectric relaxation method. Chin. J. Chem. Phys **21**, 270–274 (2008)
64. O. Bohnke, C. Bohnke, J.L. Fourquet, Mechanism of ionic conduction and electrochemical interaction of lithium into the perovskite lanthanum lithium titanate. Solid State Ion. **91**, 21–31 (1996)
65. A.K. Jonscher, *Dielectric Relaxation in Solids* (Chelsea Dielectrics Press, London, 1983)
66. M. Li, D.C. Sinclair, A.R. West, Extrinsic origin of the apparent relaxorlike behavior in $CaCu_3Ti_4O_{12}$ ceramics at high temperatures: a cautionary tale. J. Appl. Phys. **109**, 084106 (2011)